Angle-resolved Photoemission of the Clean InSb(100) Surface

Hem Raj Sharma

Dissertation submitted for
1998-99 Diploma Course in Condensed Matter Physics

The Abdus Salam International Centre for Theoretical Physics
Strada Costiera 11, Miramare P.O. Box 586
I-34100 Trieste, Italy

Supervisor: Prof. Massimo Sancrotti

September 1999

Acknowledgement

I would like to express my heartfelt gratitude to my supervisor Prof.Massimo Sancrotti for suggesting the experimental work and his constant guidances and encouragements throughout this work.

My deepest thanks go Mrs Elena Magnano for her kind help and suggestion during the whole work. I express my thanks to other members of this group especially to Mrs Marina Pivetta and Anna Refaldi for their help during this work.

I express my gratitude to Prof. Kevin Prince for providing his laboratory for this work.

I am thankful to Mrs Cinzia Cepek for providing a computer programme for a simulation.

I would like to express my sincere thanks to Prof. Subodh Shenoy (Co-ordinator, diploma programme-CMP) for his encouragement and helpful suggestions during my year's stay in ICTP.

Cooperation from my colleagues is appreciated.

My thanks also goes to UNESCO, the IAEA, Prof. M. A. Virasoro, the Director of the ICTP, Prof. Yu LU, Head of Condensed Matter Group and Ms. Concetta Mosca, Secretary of the Diploma Programme for their kind hospitality at the centre during my study at ICTP.

Abstracts

We have found the experimental surface and bulk energy band for the InSb(100)-c(2×8) reconstructed surface by using the Angle-Resolved Photoemission Spectroscopy.An He-discharge lamp was used as a source. The Low Energy Electron Diffraction (LEED) technique was used to check the crystallographic structure of the surface. The sample was prepared by a repeated cycle of Ar ion bombardment and annealing. The bulk- and surface-related states have been identified by comparing the spectra from the clean and hydrogen contaminated surface. We have found many of the obtained states are in strict similarity with the states observed in Angle-Resolved Photoemission spectra for the InSb(100)-(4×1) and the GsAs(100) surface. The periodicity shown by the LEED pattern has been compared with the periodicity obtained from the dispersion of the surface bands as well as a simulated LEED pattern.

Contents

Chapter 1

1 Introduction

1.1 General introduction

Since the surface is the termination of a bulk crystal, part of chemical bonds which constitute the bulk-crystal structure are broken at the surface, and hence surface atoms have fewer neighbors than bulk atoms. Breaking of bonds to form a surface costs energy: the so called 'surface tension'. Hence the electronic structure near the surface is markedly different from that of the bulk. Many macroscopic effects and phenomena at surface such as surface energy, adhesion forces etc. are related to this change in the electronic structure.

The general principles that determine the electronic structure of semiconductor surfaces derive from the familiar notions of local chemical bonding. In the bulk, significant covalent bond orbitals are formed from linear combination of low-lying atomic s- and p-orbitals. The highly directional sp^3 hybrid bonds that result determine the diamond and zinc blende crystal structures of most common semiconductors. Overlapping hybrid orbitals on neighboring tetrahedrally coordinated sites produces bonding and anti-bonding levels which ultimately broaden into semiconductor valence and conduction bands respectively.

The ideal surface (truncated bulk, having same periodicity of bulk lattice) of semiconductor lattice exposes hybrid orbitals that 'dangle' into the vacuum. The formation of truncated (111) surfaces creates one half-filled dangling bond orbital per surface atom perpendicular to the surface. On the (110) surface there are two atoms per unit cell, each with a tilted dangling bond orbital. The unreconstructed (100) surface unit cell contains one atom with two broken bonds tilted with respect to one another [Figure 1]. Since the areal density of dangling bonds is lower for (111)

surfaces and higher for (100) surface, surface tension is higher for (100) surfaces and lower for (111) surfaces.

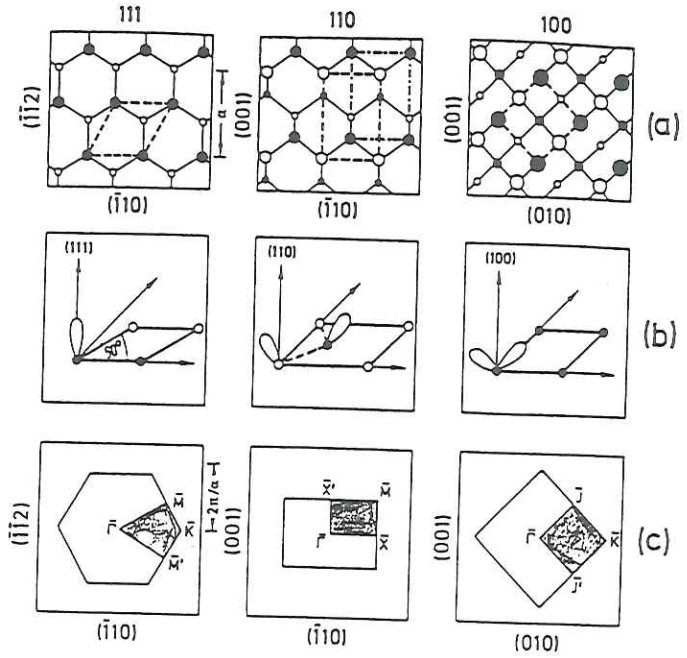

Figure 1.1 Crystallography of the non-reconstructed three low-index surfaces of the zinc blende lattice (sp^3-bonded). (a) top view, small symbols denote deeper lying atoms. Possible unit meshes are indicated by broken lines. (b) Schematic plot of the dangling-bond orbitals occurring on the different surfaces. (c) Corresponding ideal surface Brillouin zone with conventional labeling.

When the surface bonds are broken, hybrid bonding and anti-bonding states revert to their original single atom hybrid energy values. A fraction of surface localized

levels may lie in the bulk-band gap or be degenerate with bulk band states. The interaction among these surface states yields a dispersive energy band which is small (with respect to the dispersion of the bulk-states) due to reduced orbital overlaps. Particularly at (100) surfaces, two surface-state bands appear in the fundamental gap region, corresponding to two dangling bonds. The non-negligible interaction between two dangling bonds produce the splitting between two surface bands.

Since the bulk covalent bonding is highly directional and inflexible, it costs too much energy to locally rearrange the electron wave functions at the surface as required by dangling bonds, without major lattice readjustments. 'Reconstruction' reduces dangling bonds as much as possible, therefore all semiconductor surfaces are essentially reconstructed, and display a variety of complicated reconstructions. Reconstruction depends upon preparation conditions. For example, Si(100) presents a (2×1) reconstruction when the crystal is cleaved at room temperature (RT) while a (1×1) reconstruction is obtained if cleaved at very low temperature ($T < 20K$). After annealing to temperature higher than about 400°C a (7×7) reconstruction occurs, indicating an extremely long-range periodicity [1].

The most frequently used surface of compound semiconductors in device technology is the (100) surface. Parallel to this surface, the zinc blende crystal is built up of alternating layers of anions and cations, and the ideal unreconstructed surface is therefore electrostatically unstable. Different stoichiometries and reconstructions occur depending on preparation technique. When using sputtering and annealing the (100) surface is generally cation-rich. Anion termination can be achieved by using, e.g. molecular beam epitaxy (MBE). Because of the close relationship between geometric and electronic surface structure a detailed characterization of all reconstructions are of both fundamental and technological interest.

InSb surfaces have been intensively used for heteroepitaxial growth of α-Sn starting from the pioneering work by Farrow *et al* [2]. Heteroepitaxial growth is favored when a good surface lattice matching between the adlayer and the substrate is

achieved. In this respect, InSb is a good candidate, presenting a lattice parameter of 6.4798 $\AA$ at room temperature closely lattice matched to that of α-Sn (6.489$\AA$).

Due to the different gap values in the infrared (IR) energy region, α-Sn/InSb interfaces might be useful for application in IR optoelectronic devices.

1.2 InSb(100) surface

InSb presents the zincblede structure [Figure 1.2(a)] with a band gap 0.17 eV at RT. The (100) and the (111) surfaces are polar while the (110) surface is non-polar. The crystal structure of ZnSe is presented in Figure 1.2(a) showing the different surface planes. We can clearly see from this Figure that (111) and (001)surfaces present Zn and Se terminated surfaces while (110) contains both Zn and Se. The analogy is true for InSb crystal. Top view of InSb(100) surface has already been presented in Figure 1.

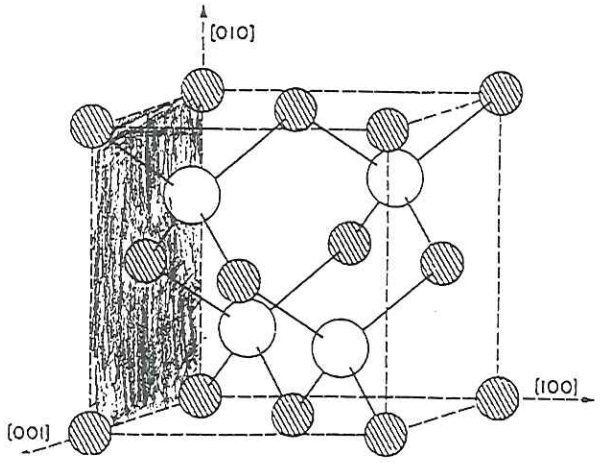

Figure 1.2 (a) Zinc blende structure of InSb (shaded area is (100) plane).

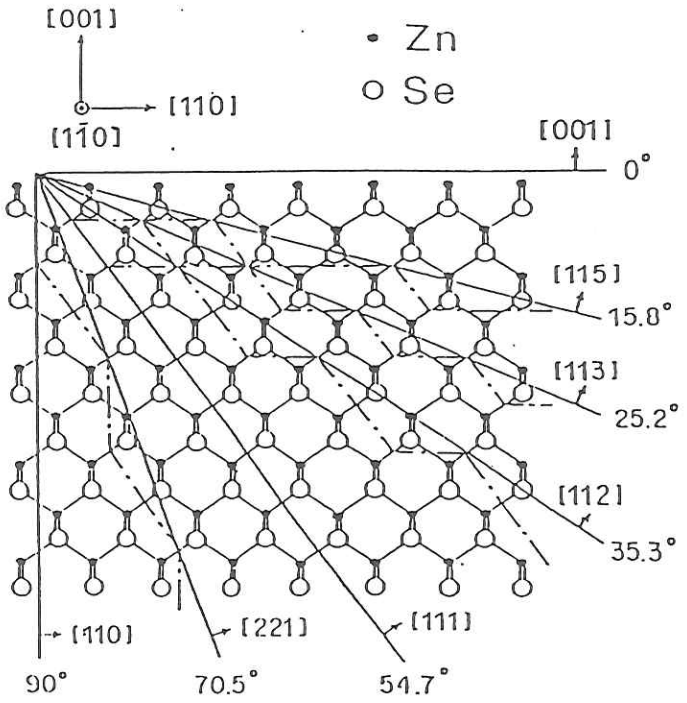

Figure 1.2 (b) ZnSe structure showing different surface planes.

RHEED measurements [3,4] identified several reconstructions of InSb(100) surface. The reconstruction of III-V semiconductors depends upon preparation conditions and the ratio of In and Sb atoms at the surface. In order of decreasing antimony concentration, the principal reconstructions are (1×1), a (4×4), a A (1×3), a c(8×2). Of these, the Sb-rich c(4×4) and In-rich c(8×2) have been the most intensively studied. There is a strong consensus that the c(4×4) reconstruction is composed of groups of antimony dimers aligned along the [110] bulk axis of an antimony terminated and largely undisturbed bulk structure. Several models have been proposed to describe the InSb(100)-c(8×2) surface structure [5-8] but there is still remains a debate about these models up to now.

In this work, we will the present electronic properties of the InSb(100)-c(8×2) surface studied by using the angle-resolved photoemossion spectroscopy (ARPS). The periodicity shown by the LEED pattern will be compared with periodicity obtained from the dispersion in the Surface Brillouin Zone (SBZ) of surface bands, as well as with a simulated LEED pattern. We will also compare the thus-obtained surface bands with InSb(100)-c(4×1) surface bands reported by Olsson *et al* [9], and with GaAs(100) as well. We will also present the spectra obtained from the hydrogen contaminated surface. We have identified the surface and the bulk states of clean surface comparing its spectra with the spectra from the hydrogen contaminated surface.

In the chapter 2 we will discuss the experimental techniques and apparatus. Experimental results will be discussed in chapter 3. Finally we will present the conclusions.

Chapter 2

2 Experimental Techniques and Apparatus

2.1 Experimental Techniques

2.1.1 Angle-Resolved Photoemission Spectroscopy (ARPS)

Phenomenology

The most important and widely used experimental technique to gain information about occupied electronic surface states, is photoemission spectroscopy. The experiment is based on the photoelectric effect. The solid surface is irradiated by mono-energetic photons, and emitted electrons are analyzed with respect to their kinetic energy. In ARPS, the emitted electrons are analyzed with respect to direction (θ and ϕ; figure 2.1.1 (a)) as well as kinetic energy. ARPS is used to investigate the dispersion of electronic bands.

Einstein's relation

$$E_{kin,max} = \hbar\omega - \phi \tag{1}$$

says that maximum kinetic energy of an electron emitted in the photoelectric effect is equal to the photon energy, minus the energy necessary to release the electron from the solid. ϕ is called the work function.

The extension of Einsten's relation to include not only the highest electrons, but all of them is

$$E_{kin,max} = \hbar\omega - \phi - E_B \tag{2}$$

where E_B = binding energy of ejected electrons referred to Fermi level E_F. Electrons deriving from valence bands can be found at binding energies of several eV while those from core levels contribute between several tens eV and several thousand eV.

The beauty of a photoemission experiment is that one sees a certain fraction of photoelectrons (so called primaries) escaping without any inelastic interaction with the solid. This fraction ranges from a few percentage to almost 100 % of photoelectric yield and can be distinguished by a higher kinetic energy and sharply structured energy distribution whereas the secondary electrons form a relatively smooth background. Another advantage of photoemission is the time scale. Typical transition times between electronic states are about $10^{-15}s$ and comparable to the escape time of photoelectrons of kinetic energy greater than few electron volts [10]. Therefore the atoms in a solid do not have time to rearrange themselves and thereby change the electronic states during the photoemission process. This is referred to as the Frank-Condon principle or the Born-Oppenheimer approximation.

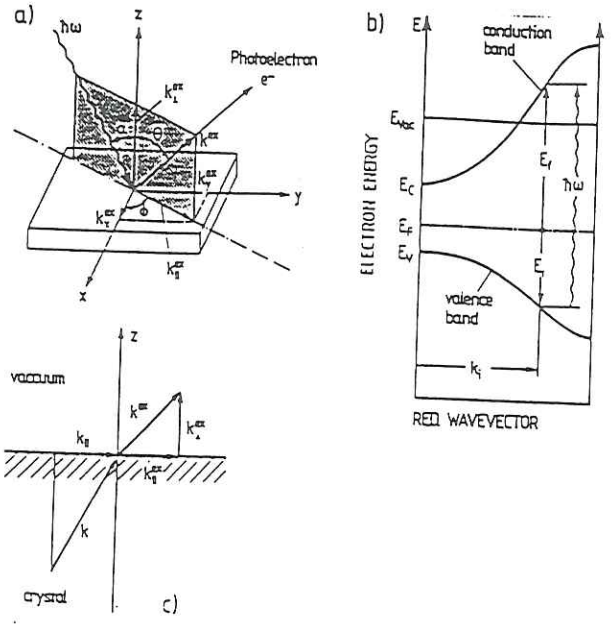

Figure 2.1.1 Description of a photoemission experiment. (a) Definition of angles and wave vectors of incident photon ($\hbar\omega$) and emitted electron (e^-). (b) Representation of the photo-excitation process in the electron band scheme $E(\mathbf{k})$ of a semiconductor. (c) Conservation of $\mathbf{k}_{||}$.

Single-particle aspects of photoemission

The less accurate but simpler and more instructive approach to the photoemission process is the so-called three-step model, in which the photoemission process is artificially separated into three independent parts:

(1) Optical excitation of an electron from an initial to final state within the crystal.

(2) Propagation of the excited electron to the surface.

(3) Emission of the electron from solid the into the vacuum.

The optical excitation of an electron in the first step is simply described by the 'golden-rule' transition probability for optical excitation,

$$W_{fi} = \frac{2\pi}{\hbar}|\langle f,\mathbf{k}|H|i,\mathbf{k}\rangle|^2\delta(E_f(\mathbf{k}) - E_i(\mathbf{k}) - \hbar\omega)$$

$$= \frac{2\pi}{\hbar}\, m_{fi}\, \delta(E_f - E_i - \hbar\omega) \qquad (3)$$

To a first approximation, direct transitions with nearly unchanged $\mathbf{k}$ are taken into account between the initial and final Bloch states $|i,\mathbf{k}\rangle$ and $|f,\mathbf{k}\rangle$. In fact, a UV photon adds negligible momentum to the electron momentum. The perturbation operator H is given by the momentum operator $\mathbf{P}$ and the vector potential $\mathbf{A}$ of the incident electromagnetic wave (dipole approximation).

$$H = \frac{e}{2m}(\mathbf{A}\cdot\mathbf{P} + \mathbf{P}\cdot\mathbf{A}) \qquad (4)$$

The δ-function in equation (3) describes the energy conservation in the excitation of an electron from a state $E_i(\mathbf{k})$ into a state $E_f(\mathbf{k})$ of the electronic band structure [Figure 2.2.1(b)].

The internal electron current density directed towards the surface with an energy E and a wave vector around $\mathbf{k}$ is therefore,

$$I^{int}(E,\hbar\omega,\mathbf{k}) \propto \sum_{f,i} m_{fi}\; f(E_i)\; \delta(E_f(\mathbf{k}) - E_i(\mathbf{k}) - \hbar\omega)\; \delta(E - E_f(\mathbf{k}) \qquad (5)$$

where $f(E_i)$ is the Fermi distribution function which ensures the initial state E_i is occupied.

The second step is the propagation of electrons towards the surface which is described by the transport probability,

$$D(E, \mathbf{k}) \propto \lambda(E, \mathbf{k}) \tag{6}$$

Where $\lambda(E, \mathbf{k})$ is the inelastic mean free path of electrons, which depends upon material and kinetic energy of electrons. Its value is typically between 5 and 20 $\AA$, thus limiting the information depth to this spatial region. The dependence of λ on the kinetic energy is shown in Figure 2.1.1 (d)

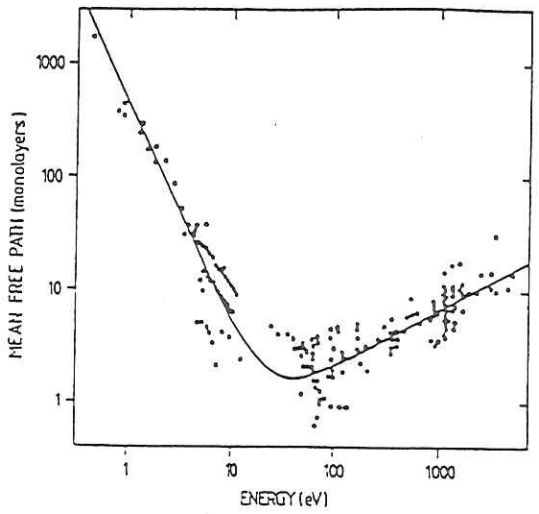

Figure 2.2.1(d) Mean free of electrons in solids as a function of their energy, a compilation of variety of experimental data.

The third step, the transmission of the photo-excited electrons through the surface can be considered as the scattering of a Bloch electron wave from the surface

atom potential with translational symmetry parallel, but not normal to the surface. Because of the 2D translational symmetry, the transmission of the electron through the surface into vacuum requires conservation of its wave-vector component parallel to the surface [Figure 2.2.1(c)].

$$\mathbf{k}_{||}^{ext} = \mathbf{k}_{||} + \mathbf{G}_{||} \tag{7}$$

The wave-vector component $\mathbf{k}_{||}^{ext}$ is independent from known experimental parameters.

$$\mathbf{k}^{ext} = \sqrt{\frac{2m}{\hbar^2} E_{kin}} \sin\theta \approx 0.512\sqrt{E_{kin}} \sin\theta \tag{8}$$

where $\mathbf{k}_{||}^{ext}$ is in A^o and E_{kin} is in eV and ϕ = angle between the photoelectrons trajectory and the surface normal. $\mathbf{G}_{||}$ is a reciprocal lattice vector.

Bulk and Surface states

Bulk states and surface states are observed in photoemission experiments and have to be distinguished from each other. One criterion for surface states is that emission from real surface states must fall into a bulk-band gap, which can be checked by comparison to calculated or measured bulk band structure. Secondly, surface states are two dimensional. A surface state shows therefore no dispersion when $\mathbf{k}_{\perp}$ (component of wave vector normal to the surface) is varied. This can be verified by changing the photon energy in photoemission while keeping $\mathbf{k}_{||}$ constant. The third criterion is the dependence on the condition of the surface. Since a surface state is localized at the surface atomic layer, a change sensitive to a reaction occurring at surface can be expected. Such a change can easily be accomplished by chemisorption (generally with hydrogen or oxygen) leading to the the removal of surface states.

2.1.2 Low Energy Electron Diffraction (LEED)

Elastic scattering or diffraction of electrons is the standard technique in surface science for obtaining structural information about surfaces. The method is applied to

check the crystallographic quality of a freshly prepared surface and as a means of obtaining new information about atomic surface structure. The periodicity of surface, i.e. surface unit mess, is obtained from the spot separation of the diffraction pattern. Since the diffraction pattern corresponds essentially to the surface reciprocal lattice, the reverse transformation yields the periodicity in real space.

The basis of the interference of electrons at a crystal surface is the de Broglie equation $\lambda = \frac{h}{mv}$. In the case of wave scattering at an array periodic in one dimension, constructive interference takes place if the scattered waves from neighboring lattice points have path differences of multiples of the wavelength λ. If the primary wave strikes the surface with an incident angle φ_o, interference of the backscattered waves occurs in directions φ [Figure 2.1.2], where φ is given by the condition

$$a(sin\varphi - sin\varphi_o) = n\lambda$$

a is the distance between the periodically arranged scatterers and n an integer denoting the order of diffraction.

An arrangement of lattice points which is periodic in two dimensions may be considered as an ensemble of parallel rows of scatterers with directions $[h'k']$ and mutual distances $d_{h'k'}$. In this case interference maxima are to be expected in directions given by

$$n\lambda = d_{h'k'}(sin\varphi - sin\varphi_o)$$

For normal incident of the primary electrons (φ_o=0), this equation simplifies to

$$sin\varphi = \frac{n\lambda}{d_{h'k'}} \approx \frac{n}{d_{h'k'}}\sqrt{\frac{1.5}{U}}$$

with the electron energy U in eV and $d_{h'k'}$ in nm. Each set of atomic rows $h'k'$ will therefore give rise to a series of diffraction maxima nh', nk' with varying order of diffraction n.

The advantage of this simple treatment is that a complete description of the direction of the interference maxima is given. The direction can be observed in a

typical LEED apparatus, and this allows the d_{hk} to be determined and therefore yield the geometry of the unit cell.

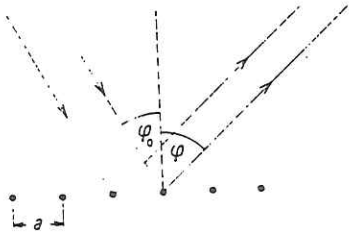

Figure 2.1.2 Scattering of a plane wave at a one dimensional periodic lattice.

In the next subsection we will mainly focus on the instrumentation and experimental methods. We will present our experimental chamber, LEED apparatus and Electron Energy Analyzer. The preparation of the sample, measurement of spectra from clean surface and hydrogen contaminated surfaces will be also discussed.

2.2 Experimental Apparatus

The experiment was performed at the 'Prototipo' laboratory at the AREA SCIENCE PARK in Trieste in a Ultra High Vacuum (UHV) Chamber at a base pressure of about 10^{-10} mbar. The analysis of surfaces must be carried out at this pressure in order to avoid the contaminations on the sample during the measurement. A description of the main chamber and some technical details about main instruments are presented below.

2.2.1 Experimental UHV Chamber

The experimental chamber of stainless steel [Figure 2.2.1] is equipped with a He discharge lamp, a hemispherical angle-resolved analyzer, a LEED apparatus, an ion gun to prepare the sample, a quadrupole mass spectrometer to monitor the residual gas in the chamber, a four degree of freedom manipulator and a combination of rotary pump and turbo molecular pump to evacuate the chamber. A Insb(100) wafer is mounted on the manipulator by means of Tantalum clips.

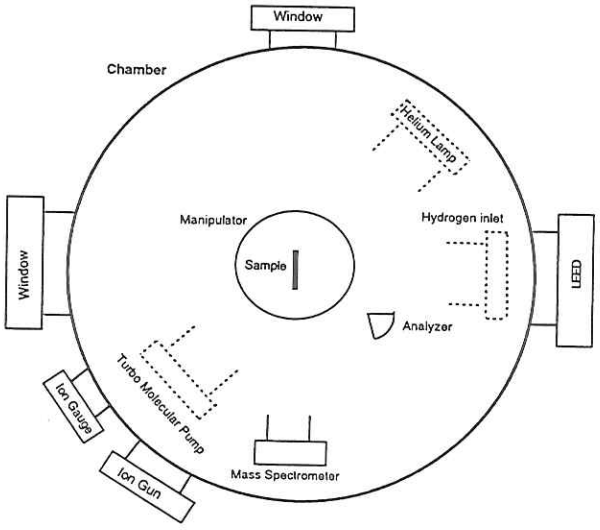

Figure 2.2.1. Experimental UHV Chamber.

2.2.2 LEED

Four grid LEED SPECTALEED OMICRON system [Figure 2.2.2] was used to check the crystallographic structure of the sample surface. A collimated and monoenergetic electron beam (with energy typically varying between 20 eV and 500 eV) from the electron gun located at the center of the fluorescent screen hits the sample. By means of the hemispherical concentric grids, the elastically scattered electrons are accelerated onto the fluorescent screen, held at positive potential of a few kilovolt, with the adequate energy to excite the phosphorus.

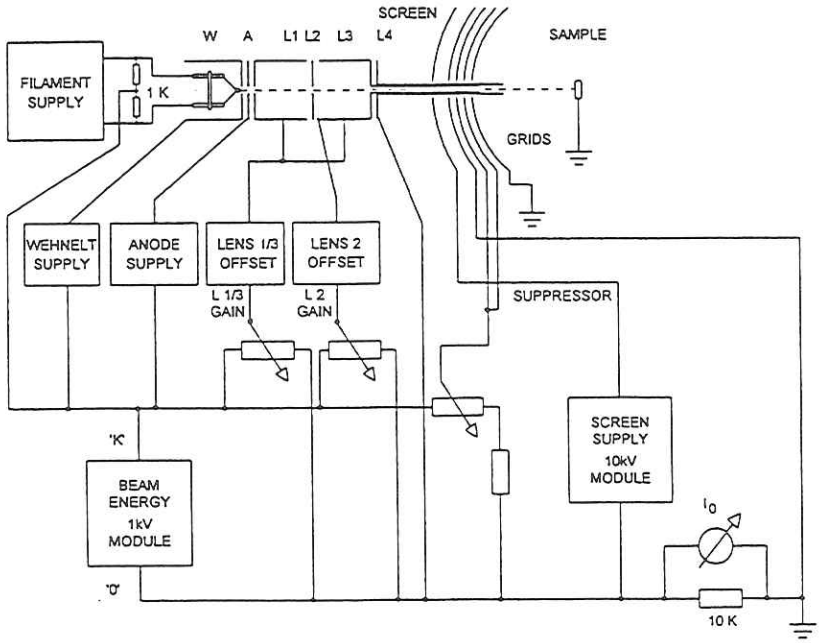

Figure 2.2.2. Schematic diagram of the SPECTALEED control unit.

2.2.3 Electron Energy Analyzer

A hemispherical VSW analyzer was used to detect the energy distribution of electrons emitted from the sample. The analyzer is movable on a two goniometer system in order to have possibility to measure angle-resolved spectra or momentum distribution of emitted electrons. A scheme of the analyzer is shown in Figure 2.2.3.

This type of analyzer is based on the use of an electrostatic field applied between the two concentric metallic hemispheres. The electrons of energy E_o passing through the entrance slit are focussed onto the exist slit if the following relation between the potential difference U_k across two hemispheres of radii R_1 and R_2 and E_o is fulfilled.

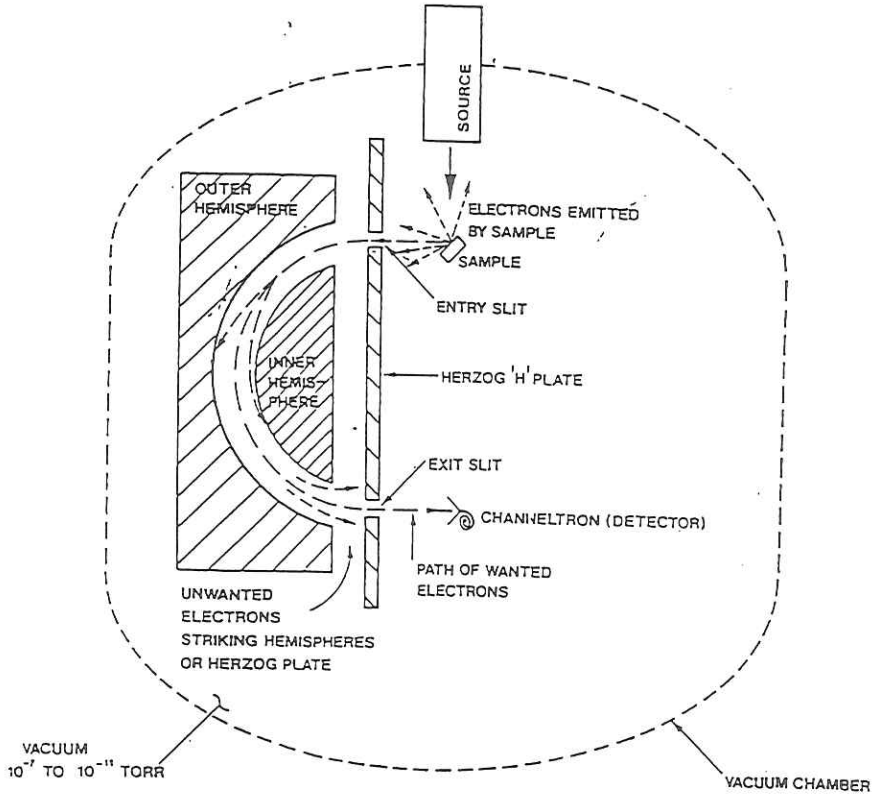

Figure 2.2.3 Schematic diagram of the electron energy analyzer.

$$U_k = \frac{E_o}{e}(\frac{R_1}{R_2} - \frac{R_1}{R_2}),$$

e electronic charge.

The energy resolution depends upon the geometric characteristic of the analyzer and the transmission energy of the electrons:

$$\delta E = \frac{\omega}{r} E_o$$

where r is the mean radius of analyzer and ω be the width of the entrance slit. Values of E_o and ω can be varied to have the desired energy resolution.

In order to have constant resolution over the entire spectrum, the pass energy (energy of transmitted electrons) E_o is kept constant throughout the measurements by accelerating and deaccelerating the incoming electrons. The angular resolution of an analyzer during measurement was 2^o and energy resolution was 0.15 eV.

2.2.4 He-Source

The photoelectrons were excited by using the radiation from a He discharge lamp.

Helium gas at some tenths of a millibar is excited in a discharge:

$$He(S_o^1) \rightarrow He*, He^+$$

Fluorescence from the (1s,2p) states occurs with photon emission via

$$He(P_1^1) \rightarrow He(S_o^1) + h\nu(21.21eV)$$

The emission spectrum is dominated by the so-called He-I radiation. Driven at lower pressures and higher currents, emission from a resonance line of ionized He^+ is increased corresponding to a photon energy of 40.8 eV.

The measurements were performed using He-I radiation (21.21 eV) and with an operating pressure of about 1×10^{-8} mbar.

Preparation of the sample

The InSb (100) sample surface was prepared by repeated cycles of sputtering and annealing. The sputtering procedure consists of the admission of Ar gas into the chamber up to a pressure 10^{-6} mbar. The crystal surface is bombarded by an Ar ion current produced by ion gun positioned in front of the crystal surface. Ar ions are produced by electron impact with gas atoms. The ions are then accelerated by a voltage of 500V. Hence contaminants at the sample surface can be removed. After sputtering, the sample was annealed up to 350°C for two minutes by Ohmic heating to remove embedded and adsorbed noble gas. Annealing process also segregates the impurities (if present) from bulk to surface, therefore sputtering and annealing cycles were repeated several times until sharp c(8×2) reconstructed surface was obtained. The surface crystallography was monitored in each cycle by LEED. Only flashing of sample at 350°C for 1 minute was sufficient to obtain this reconstruction in later experiments.

In order to measure the spectra from contaminated sample, the clean surface was exposed to hydrogen by admitting molecular hydrogen to the chamber through a leak valve and activated by a hot (about 2000 K) tungsten filament which was in line of sight of the sample at a distance of about 5cm.

Measurements were performed keeping the angle of incident photons equal to 45° with respect to the surface normal. Spectra were recorded along ΓJ and $\Gamma J'$ directions of the ideal (1×1) SBZ for a number of angles by varying the angle of detection of emitted electrons.

Chapter 3

3 Experimental Results and Discussions

This Chapter is divided in to four Sections. In the first Section, we will discuss about the surface Brillouin zone of ideal and reconstructed surfaces supported by LEED pattern. In the second Section we will present the photoemission spectra of the InSb(100)-c(2×8) surface and compare them with the spectra for InSb(100)-(4×1) surface and GaAs(100) surface. The spectra from hydrogen contaminated surface will be presented in third section and hence we will identify the bulk and surface states. Finally we will present the experimental surface and bulk energy band dispersion of the c(2×8) surface.

3.1 The Surface Brillouin Zone and the LEED picture

We present the LEED picture of a InSb(100) sample freshly prepared by a repeated cycle of annealing and Ar ion bombardment [figure 3.1(b)]. The picture clearly shows the pattern of typical c(2×8) reconstruction. Before getting this sharp LEED pattern, there were strips instead of the dim spots in the left and right columns of middle bright column of spots. The absence of these dim columns leads to the (1×4) reconstruction. The Figure 3.1(a) is the bulk (1 × 1) and reconstructed c(2×8) structure in reciprocal space obtained by a simulation. The superposition of the simulated c(2×8) structure to the LEED picture [Figure 3.1(c)] shows that all obtained diffracted spots (of course some spots are missing, reason of which can not be described here) lie in c(2×8) lattice points. This is the strong support of this reconstruction of our sample.

Figure 3.2 illustrates the reconstructed (1×4) and c(2×8) structures in the reciprocal space and their SBZ's. The InSb lattice constant is a = 6.479 $\mathring{A}$, so for the (1×1) SBZ, $\Gamma K_{(1\times1)} = \frac{2\pi}{a} = 0.97\ \mathring{A}^{-1}$ and $\Gamma J_{(1\times1)} = \Gamma J'_{(1\times1)} = \frac{\Gamma K_{(1\times1)}}{\sqrt{2}} = 0.686$

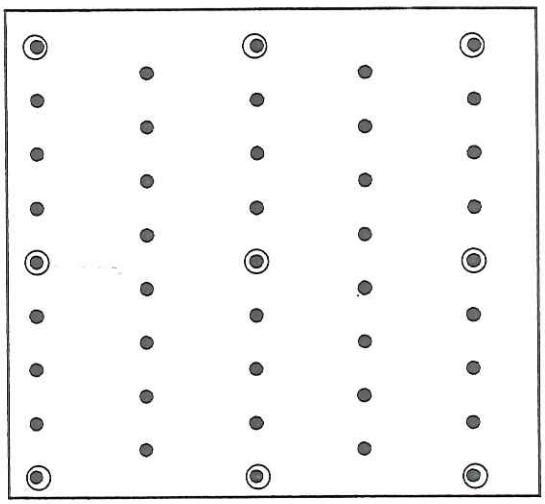

(a)

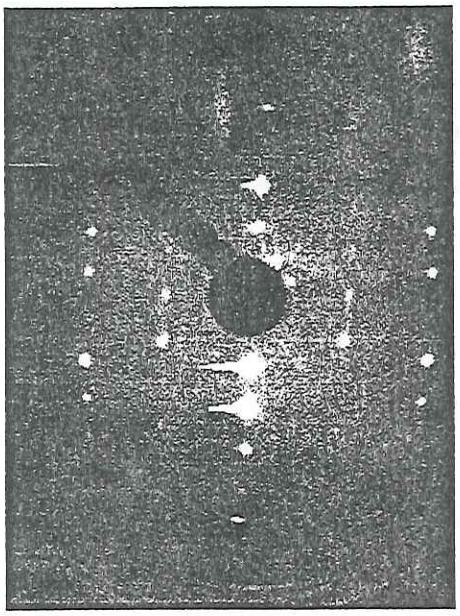

(b)

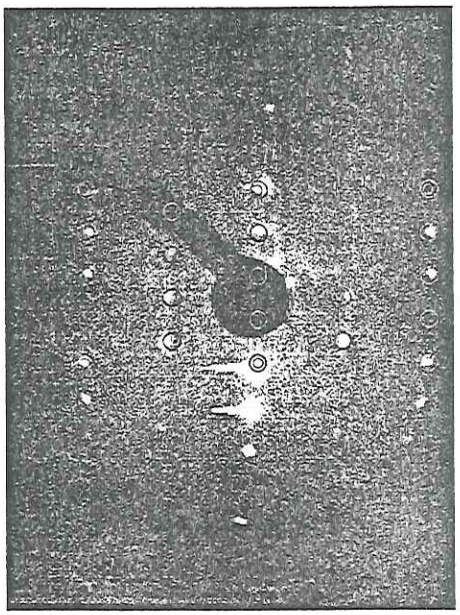

(c)

Figure 3.1. (a) Simulated c(2x8) reconstruction in reciprocal space (open circles are bulk position), (b) LEED picture , (c) Superposition of LEED picture with the simulated c(2X8) structure.

$\AA^{-1}$. Hence $\Gamma J_{c(2\times8)} = 0.343\ \AA^{-1}$. We have measured the spectra along $\Gamma J_{(1\times1)}$ and $\Gamma J'_{(1\times1)}$ symmetry lines. Along $\Gamma J_{(1\times1)}$ direction, we have detected the spectra up to 20^o in 2^o interval starting from normal emission. For typical value of $E_{kin} = 14$ eV, the relation $\mathbf{k}_{||} = 0.512\ \sqrt{E_{kin}} sin\theta$ gives $\mathbf{k}_{||} = 0.655\ \AA^{-1}$ which is approximately four times $\Gamma_{c(2\times8)} J_{c(2\times8)}$. Therefore we should expect four fold periodicity in the energy band dispersion of the c(2×8) surface measured up to this angle. The situation is different along the $\Gamma J'_{(1\times1)}$ direction. To move from $\Gamma_{(1\times1)}$ of first BZ to $\Gamma_{(1\times1)}$ of the second BZ ($\mathbf{k}_{||} = 1.37\ \AA^{-1}$), We have to detect the emission up to $\approx 45^o$ (for $E_{kin} = 14$ eV) from normal emission. We have moved the analyzer through 40^o consequently we expect one fold periodicity in the surface energy band dispersion along the $\Gamma J'_{(1\times1)}$ symmetry line. It is clear from Figure 3.2(b) that (1×4) SBZ and c(2×8) SBZ have the same symmetry along the $\Gamma J_{(1\times1)}$ direction but they differ along the perpendicular direction. Hence, the surface energy band dispersion along the $\Gamma J_{(1\times1)}$ direction for (1×4) and c(2×8) should have the same periodicity (provided all other conditions, i.e. experimental resolution etc., are not changed). The bulk SBZ has the same symmetry in both directions.

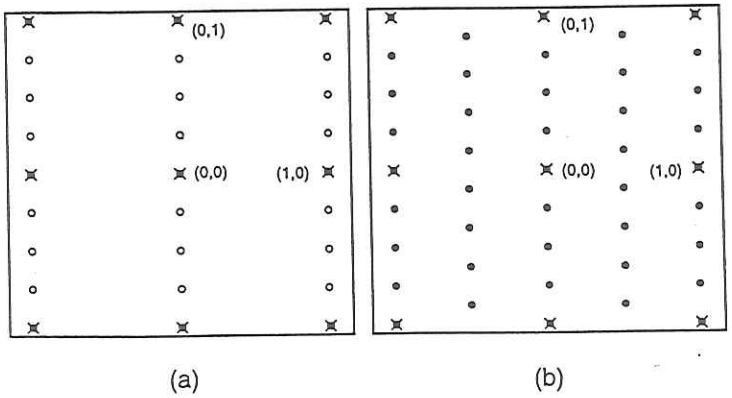

Figure 3.2 (a) Structure of (1×4) reconstructed surface in reciprocal space (RS) (b) Structure of c(2×8) reconstructed surface in RS.

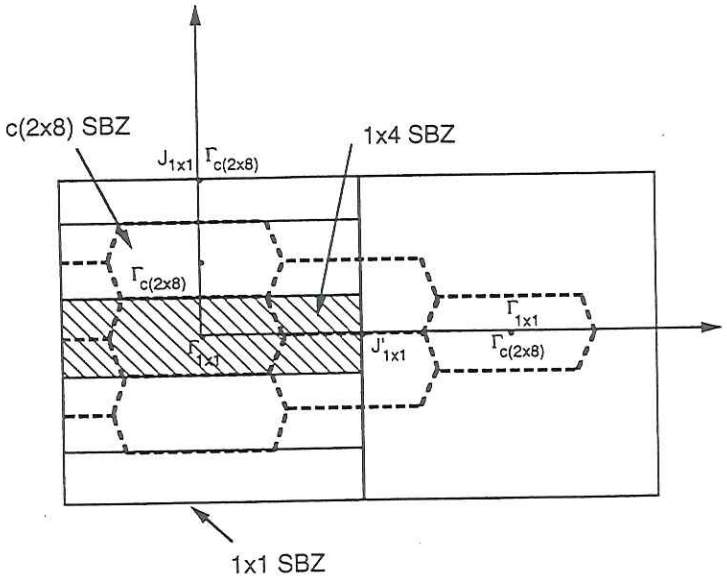

(c)

Figure 3.2 (c) SBZ of ideal surface, (1×4) reconstructed surface (shaded) and c(2×8) reconstructed surface (dashed boundary).

3.2 Photoemission Spectra

In Chapter 1 we defined surface states as those electronic quantum states related to surface atoms and falling in energy gaps of the bulk band structure projected onto the surface plane of interest. However, surface-related states can also be some time degenerate in energy with bulk Bloch states. If this happens, these states are referenced to as surface resonances. A specific band related to surface atoms can be partially dispersing in a projected bulk gap and partially dispersing over allowed bulk band structure. An associated significant difference between real surface states and surface resonances is that the associated wave functions are highly localized along the z-direction in the former case while they can be delocalized along the z-direction in the latter case this being due to a resonant coupling between the

surface-related feature and bulk Bloch states. Keeping in mind this difference, it is in any case usual to speak about surface states whenever electronic states are directly related to surface atoms. Hereafter, we will define surface states consistently with this assumption.

The obtained angle-resolved photoemission spectra with $\mathbf{k}_{||}$ lying on the symmetry lines $\Gamma J_{(1\times1)}$ and $\Gamma J'_{(1\times1)}$ for different angles of emission are shown in Figure 3.3. The energies of the photoelectrons are given with respect to the Fermi level E_F, which was measured on a tantalum foil in electric contact with the sample. From Figure 3.3 it is clearly seen that all the spectra are non metallic and contain sharp peaks and shoulders. We have identified the states $S_1 - S_4$ as surface states while the states $B_1 - B_3$ as the bulk states by comparing the spectra from clean and hydrogen contaminated surface which will be described in the next section.

The peak, designated B_1, in spectra along both direction at 4.4 eV for normal emission ($\theta = 0$) disperses while moving off-normal towards 5 eV. The photoemission spectra of InSb(100)-(4×1) surface acquired with photon energy equal to 23 eV also contain the same kind of peaks with energy 5 eV from E_F for normal emission [Figure 3.4]. Different peak positions for normal emission in (4×1) and c(2×8) spectra is due to the different photon energy of excitation. Recall we have used the photon energy of 21.21 eV. These peaks in (4×1) spectra have been identified as being due to bulk states by comparing them with theoretical calculations. The same nature of the peaks in the spectra from (4×1) and c(2×8) reconstructed surfaces is the further approval of B_1 as bulk state considering the bulk states do not depend on the specific surface reconstruction.

In both panels of the Figure 3.3 all spectra show a weak stationary bump at about 6 eV (±1.5 %).A similar feature is also seen at about ≈ 6.1 eV in the photoemission spectra taken for InSb(100)-(4×1) surface with photon energy 23 eV [Figure 3.4]. This energy corresponds to the X_6 critical point [5.97 eV] shown by pseudo-potential calculation [10]. The spectra from the GaAs (001)-(2×4) surface also present the

same stationary feature of peaks (also independent with photon energy) at energy 6.7 eV corresponding to the X_3 critical point [12].

Similarly the shoulder B_3 at the immediate left of the prominent peak S_2 is more dispersive and appears nearly for all angles along the $\Gamma J_{(1\times1)}$ direction while along the $\Gamma J'_{(1\times1)}$ direction only for near normal emission. The photoemission spectra from GaAs(100) [14] also show the peak at 2.7 eV which was identified as a bulk state by exposing the clean surface to hydrogen and oxygen. We will compare the spectra obtained from the hydrogen contaminated of InSb(100) and GaAs(100)surfaces in the next section.

Another prominent peak S_2 in the spectra along the $\Gamma J_{(1\times1)}$ direction disperses with maximum energy at 1.25 eV for normal emission (Γ point) and minimum energy at 1.71 eV for the angle 12^o ($k_{||} = 0.333\ \AA^{-1}$) which corresponds to the Γ point of the second Brillouin zone of the c(2×8) surface. The dispersion of this state shows the clear periodicity in the SBZ which is discussed in section four in detail. Nearly similar but not so clear periodic peaks are also obtained for the (4×1) surface and identified as surface related states from the fact these peaks were independent of the photon energy.

The states S_1 and S_3 appearing as shoulders of S_2 are the other surface states as in strict similarity with the (4×1) reconstructed surface. Besides $S_1 - S_3$ states, we have observed more shoulders than in (4×1) surface. The shoulder S_4 closer to the Fermi level is observed for almost all angles along $\Gamma J_{(1\times1)}$ while in $\Gamma J'_{(1\times1)}$ they appear in near normal emission. The shoulder designated S_5, appears for angles $8^o, 10^o$ and 12^o ($k_{||} = 0.27$-$0.404\ \AA^{-1}$) along the $\Gamma J_{1\times1})$ direction and for angle 24^o along $\Gamma J'_{1\times1}$ direction. Since back folding of the (1×1) SBZ into the c(2×8) SBZ would yield more surface states than into (4×1) SBZ, the observation of more surface states in the c(2×8) is reliable. The states S_4, S_5 and B_3 typically appear in the c(2×8) reconstruction.

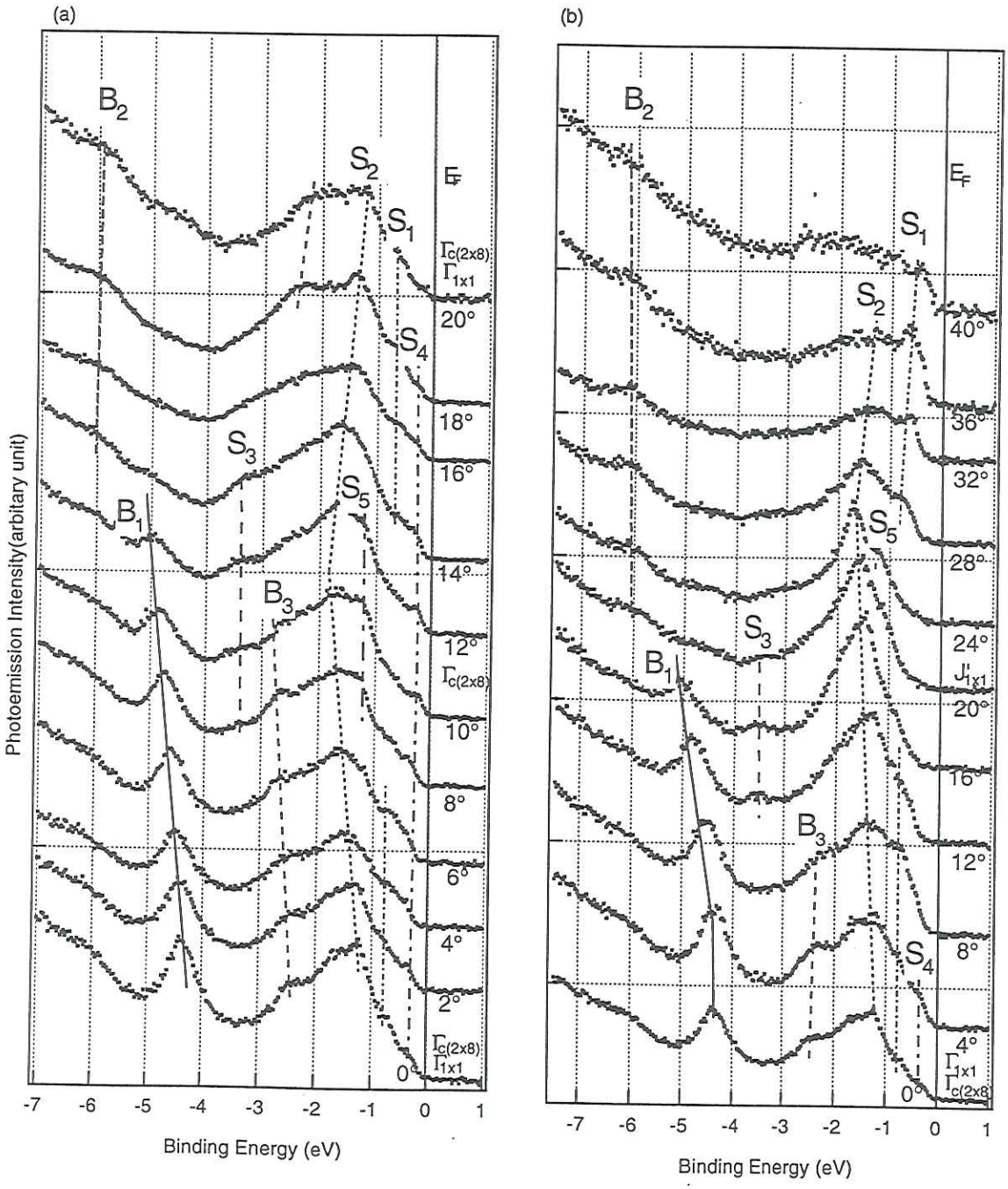

Figure 3.3 Photoemission spectra for InSb(100)-c(2×8) surface along symmetry lines $\Gamma J_{1\times1}$ and $\Gamma J'_{1\times1}$ for a certain number of emission angles.

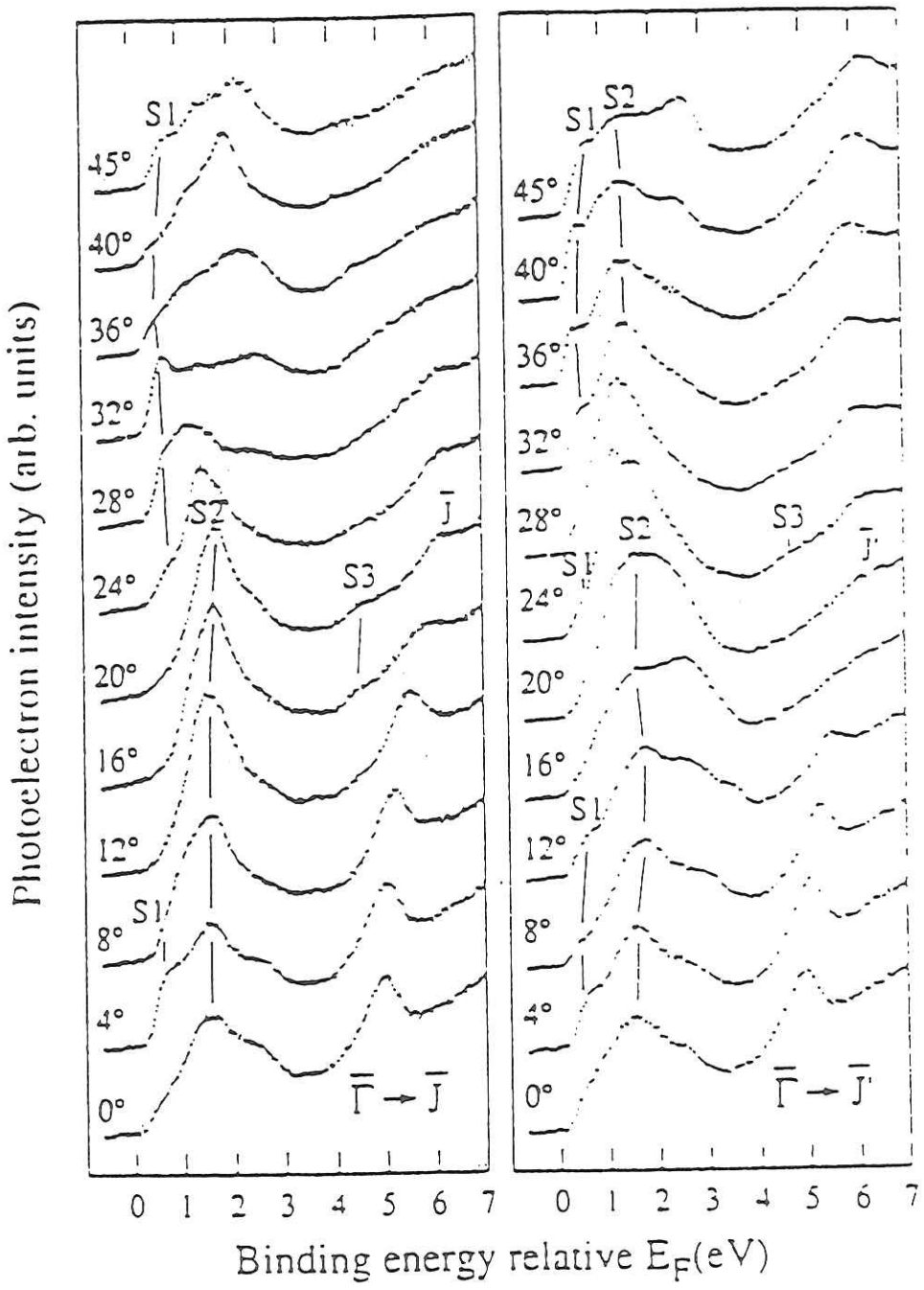

Figure 3.4 Photoemission spectra for InSb(100)-(4×1) surface along symmetry lines $\Gamma J_{1\times1}$ and $\Gamma J'_{1\times1}$ for a certain number of emission angles [9].

3.3 The Spectra from Hydrogen-contaminated Surface

In Figure 3.5(A) we show the spectra taken at normal emission. Spectrum (a) was obtained from the clean c(2×8) surface. To provide an indication of the origin of the various peaks the surfaces were subjected to different exposures of hydrogen. Spectra (b)-(e) were obtained by exposing the clean surface to different amount of hydrogen as indicated in each spectrum of Figure 3.5(A). The values for the exposures are given in Langmuirs, where 1L corresponds to 10^{-6} torr s. The surface exposed to 10^3 L of hydrogen presented the sharp (1×4) LEED pattern while sharp (1×1) LEED pattern was observed on the surface exposed to 10^4 L of hydrogen. The strips were seen in alternative columns of the LEED picture of the surface exposed to the 5×10^2 L of hydrogen leading to the (1×4) reconstruction.

The emission near the Fermi edge measured on the clean surface (a) starts diminishing after the exposure to 5×10^2 L of hydrogen (b) and it is completely disappeared for the 10^4 L exposure (e). The emission related to S_1 and S_4 clearly seen in the clean surface (a) is completely absent in the spectrum (e). This response to hydrogen indicates strongly that the shoulders S_1 and S_4 can be interpreted as surface related states. The intensity ratio between the prominent peak S_2 and its shoulder B_3 at higher binding energy (around at 2.5 eV) gradually decreases while increasing the amount of hydrogen. The dominant peak S_2 in the clean surface (a) is completely attenuated when the clean surface is exposed to 10^4 L of hydrogen (e). The removal of the prominent peak S_2 on the hydrogen exposure clearly indicates that the surface-related character of peak S_2. The shoulder B_3 remains unchanged in all treatment indicating it is bulk-related. We have presented the photoemission spectra from GaAs(100) surface for normal emission in Figure 3.6 [14]. The spectra were obtained from the surfaces after different treatments. Details can be found in corresponding reference. The peak near 2.7 eV is not influenced by any treatments indicating the bulk related state. This bulk related state may have the same reason of origin in III-V semiconductors.

The Figure 3.5(B) shows the spectra measured at polar angle 16^o out of Γ for increasing doses of hydrogen as above (Figure 3.5(A)). Considering these five spectra, it is apparent that the peak at about 5 eV binding energy is not influenced by any of the treatments and may be reasonably ascribed to a bulk state. Comparing the spectra (a) and (e), we can notice that the emission in the range between the Fermi

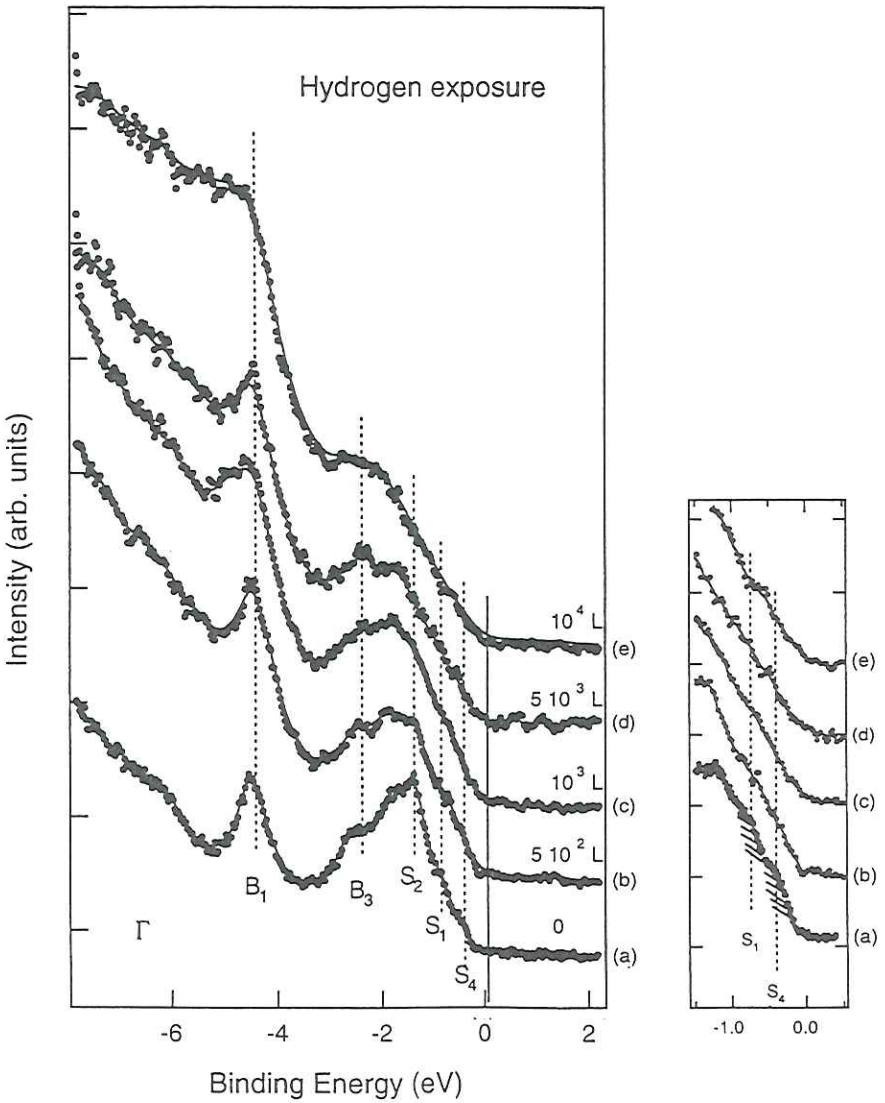

Figure 3.5(A) Photoemission spectra for InSb(100) surface at normal emission for different doses of hydrogen as indicated in each spectrum.

edge and 3 eV binding energy is strongly reduced and the remaining emission at this energies is probably related to bulk states. This consideration is supported by the observed (1×1) LEED pattern. We have already mentioned that the (1×1) LEED pattern was observed from the surface exposed to 10^4 L of hydrogen (e).

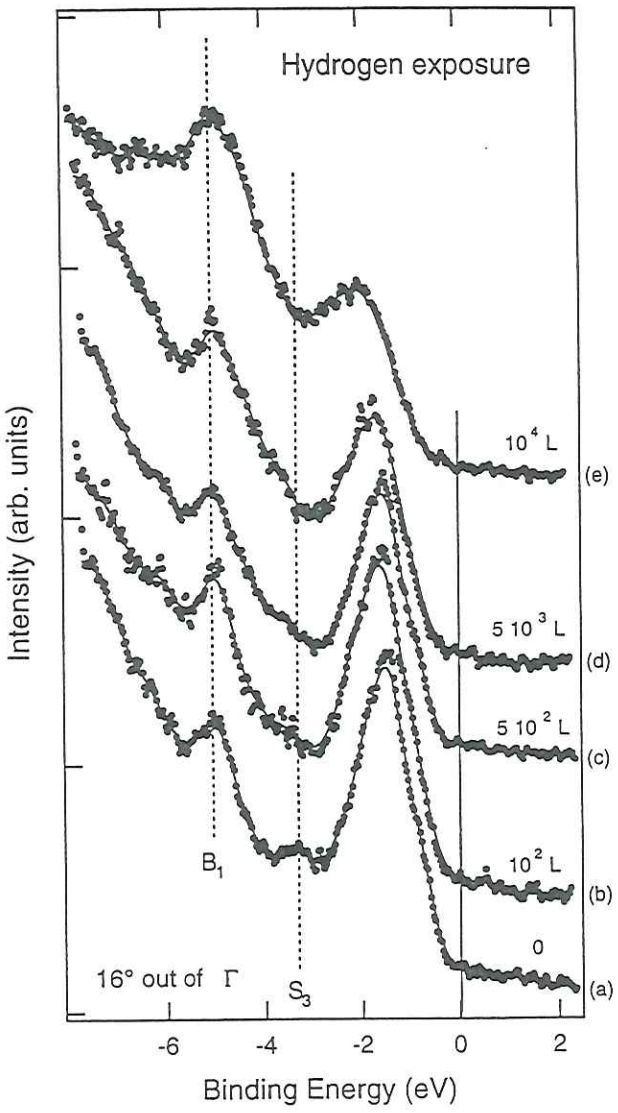

Figure 3.5(B) Photoemission spectra for InSb(100) surface for 16° polar angle out of Γ for different doses of hydrogen as indicated in each spectrum.

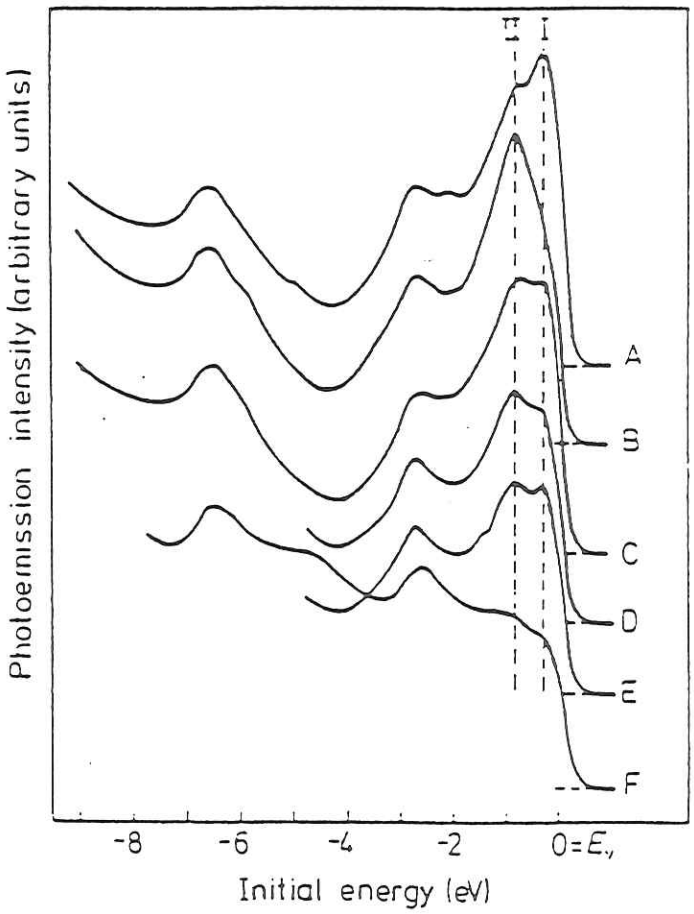

Figure 3.6 Photoemission spectra for (001)GaAs taken at normal emission. Spectra A and B were measured from (4×2) Ga-stable and (2×4) As-stable surfaces respectively, at $\sim$ 300 K. Spectra C-F were measured after: C heating a (2×4) to 750 K in vacuo for a minute; D exposure of a (2×4) surface to 2×10^4 L H_2 at 300 K; E exposure to 7.5×10^4 L H_2 at 300 K; F exposure of a (4×2) surface to 10^5 L O_2 at 300 K [14].

3.4 The Experimental Surface and Bulk Energy Bands

We present the experimental surface and bulk energy bands for InSb (100)-c(2×8) along the symmetry lines in Figure 3.7(a). As we described above, the energy bands

$S_1 - S_3$ are also related to the (4×1) surface. The $S_4 - S_5$ bands are typical of the c(2×8) reconstruction. We do not discuss the origin of these bands. Among these surface bands, S_2 along the $\Gamma J_{(1\times1)}$ azimuth is more interesting. The bulk band B_1 is parabolic with maximum energy 4.1 eV at Γ and it is symmetric along $\Gamma J'_{(1\times1)}$ as expected. The bulk BZ is symmetric in both directions as discussed above.

As we have seen from Figure 3.7(b), the periodicity dispersion of the band S_2 associated with more pronounced peaks in the photoemission spectra along the $\Gamma J_{(1\times1)}$ direction is twice what would be expected for the unconstructed (1×1) SBZ. The four fold symmetry clearly seen in the LEED picture could not be seen in the energy band dispersion. Most probably, the absence of four fold periodicity in the band dispersion is due to the experimental resolution. The finite angular resolution leads to an uncertainty in the component of wave vector $\mathrm{k}_{||}$. The uncertainty in $\mathrm{k}_{||}$ is given by

$$\Delta \mathrm{k}_{||} = 0.512\sqrt{E_{kin}}\left(\frac{sin\theta}{2E_{kin}}\Delta E_{kin} + cos\theta\Delta\theta\right)$$

With our experimental resolution ΔE = 0.15 eV and $\Delta\theta = 2^o$, the above relation gives $\mathrm{k}_{||} \approx 0.07\mathring{A}^{-1}$ for typical value of E_{kin} of 14 eV. The uncertainty in $\mathrm{k}_{||}$ amounts to $\sim$ 40% of the $\Gamma J_{c(2\times8)}$ Brillouin zone boundary momentum ($\Gamma J_{c(2\times8)} = 0.1715\mathring{A}^{-1}$). The finite resolution therefore makes it quite difficult to resolve the bands along $\Gamma J_{c(2\times8)}$ direction, requiring a four fold periodicity. In the work of angle-resolved photoemission spectra of the InSb(100) surface with nearly same experimental resolution as ours, Olsson et al [9] have also reported that dispersion in the SBZ of surface bands appeared to be periodic as (4×1), although the LEED pattern indicated a tendency towards a (4×2) reconstruction. The same case has been observed in the GaAs(001)-(2×4) reconstructed surface [13].

The dispersion of the band S_4, close to the Fermi level, seems to have four-fold periodicity as expected. Its band width is very narrow which falls with in our experimental error. So, we can not confirm its periodicity. We could not measure enough data for the states S_1 and S_5 to interpret them. The bands S_4 and B_3 appear

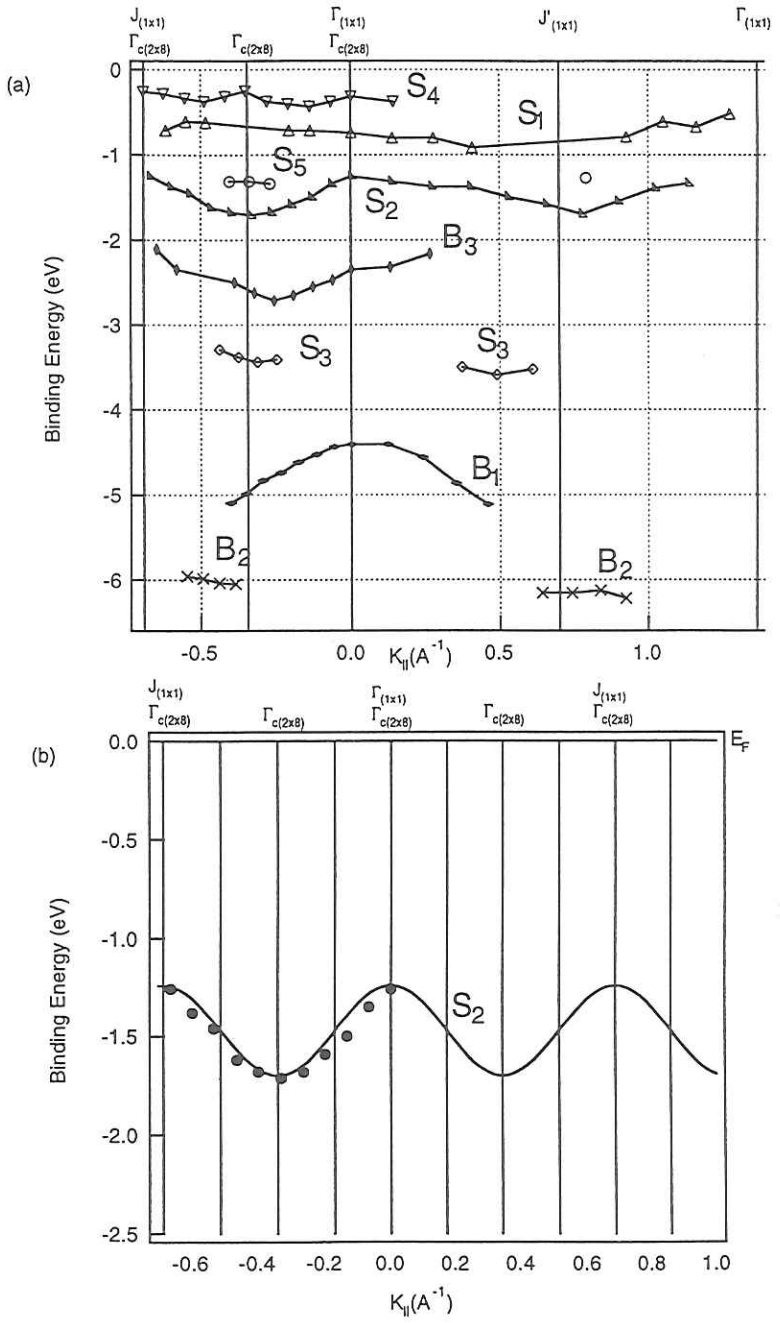

Figure 3.7(a) Experimental surface and bulk energy bands for InSb(100)-c(2×8) along the symmetry lines of SBZ, (b) Energy dispersion of the surface state S_2 of InSb(100)-c(2×8) with fitted curve.

only near the Γ point. Only S_2 and S_1 states have been observed throughout our measurements along this direction. They are not symmetric with respect to S_1 and S_2 along the $\Gamma J_{(1\times1)}$ direction. This is due to the asymmetric Brillouin zone. It can be said very roughly S_2 has one-fold periodicity and it is nearly symmetric in the $\Gamma J'_{(1\times1)}$ point as expected. S_1 also shows the same periodicity as S_2.

4 Conclusions

We have found the bulk and surface energy band dispersion of the InSb(100)-c(2×8) surface along the symmetry lines of its Surface Brillouin Zone by measuring the Angle-Resolved Photoemission Spectra. Our photoemission spectra showed eight energy states, four of which identified as surface-related states and three as bulk-related states. The spectral assignments have been made by exposing the clean sample to different amounts of hydrogen. We found more surface states at the InSb(100)-c(2×8) surface than at InSb(100)-(4×1) [9], which is consistent with the different reconstruction of our sample. The bulk state corresponding to the X_6 critical point is in strict similarity with the bulk state found at the GaAs(100) surface corresponding to X_3 critical point [14].

References

[1] H. Luth, *Surfaces and interface of Solid materials* (3rd edition-Berlin,1995).

[2] R. F. C. Farrow, D. S. Robertson, G. M. Williams, A. G. Cullis, G. R. Jones, I. M. Young and P. N. J. Dennis, J. Cryst. Growth **54** (1981) 50.

[3] K. Oe, S. Ando and K. Sugiyama, Jpn. J. Appl. Physics **19**, l417 (1980).

[4] A. J. Noreilca, M. H. Francombe, and C. E. C. Wood, J. Appl. Phys. **52**, 7416 (1981).

[5] P. John, T. Miller, T. C. Chiang, Phys. Rev. B **39**(1989) 1730.

[6] S.L. Skala, J. S. Hubacek, J. R. Tuncker, J. W. Lyding, S. T. Chou and K. Y. Cheng, Phys. Rev. B **48** (1993) 9138.

[7] D. K. Blegeisen, R. D. Bringans, S. E. Northrup and L. E. Swartz, Phys. Rev. B **41** (1990) 5701.

[8] N. Jones, C. Norris, C. L. Nicklin, P. Steadman, S. H. Baker, A. D. Jhnson and S. L. Bennett, Surface Science **409** (1998) 27-36.

[9] L. O. Olsson, Y. O. Khazmi, J. K. Ski, L. Ilver, P. O. Nilsson, M. C. Hacansson, U. O. Karlsson, Surface Science **331-333** (1995) 1176-1180.

[10] F. J. Himpsel, Advanced in Physics, **32** (1983) 1-51.

[11] J. R. Chelikowsky and M. L. Cohen, Phys.Reviw B **14** (1976) 556.

[12] P. K. Larsen, J. F. Van der Veen, A. Muzur, J. Pollmann and B. H. Verbeek, Solid State Commun. **40** (1981) 459.

[13] P. K. Larsen, J. F. Van der Veen, A. Muzur, J.Pollmann, J. H. Neave and B. A. Joyce, Phys. Rev. B **26** (1982) 3222.

[14] P. K. Larsern, J. H. Neave and B. A. Joyce, J. Phys. C: solid state phys. **12** (1779) L869